Fundamental study of nonclassical nucleation mechanisms in iron

Ou, Xiaoqin; Sietsma, Jilt; Santofimia, Maria J.

DOI
10.1016/j.actamat.2022.117655

Publication date
2022

Document Version
Final published version

Published in
Acta Materialia

Acta Materialia 226 (2022) 117655

Contents lists available at ScienceDirect

Acta Materialia

journal homepage: www.elsevier.com/locate/actamat

Full length article

Fundamental study of nonclassical nucleation mechanisms in iron

Xiaoqin Ou [a,b,*], Jilt Sietsma [a], Maria J. Santofimia [a]

[a] Department of Materials Science and Engineering, Delft University of Technology, Mekelweg 2, Delft, CD 2628, The Netherlands
[b] State Key Laboratory of Powder Metallurgy, Central South University, Changsha 410083, China

ARTICLE INFO

Article history:
Received 18 August 2021
Revised 10 January 2022
Accepted 11 January 2022
Available online 13 January 2022

Keyword:
Thermodynamics
Nonclassical nucleation
Solid state phase transformation
Iron
Molecular dynamics simulations

ABSTRACT

Nucleation is the re-arrangement of a small number of atoms in the structure of a material leading to a new phase. According to the classical nucleation theory, a nucleus will grow if there is an energetically favourable balance between the stability of the newly formed structure and the energy costs associated to the formation of strains and new phase boundary. However, due to their atomic and dynamic nature, nucleation processes are difficult to observe and analyse experimentally. In this work, atomic mechanisms and thermodynamics of the homogeneous nucleation of BCC phase in FCC iron have been analysed by molecular dynamics simulations. The study shows that atomic system circumvents the high energy barrier for homogeneous nucleation that would occur according to the classical nucleation theory by opting for alternative, nonclassical nucleation processes, namely coalescence of subcritical clusters and stepwise nucleation. These observations show the potential of nonclassical nucleation mechanisms in metals.

1. Introduction

Metallic alloys are at the core of existing and emerging technologies, of which iron alloys are the most manufactured due to their versatility and low price [1–3]. The wide range of properties that can be achieved for iron alloys are a consequence of the multiple microstructures in which these materials can be produced. These microstructures are created via phase transformations during processing, which are controlled by nucleation and growth processes [1,4]. Whereas growth phenomena are well understood, nucleation processes remain amongst the most complex and least understood phenomena in materials science.

Through development and modification for 90 years, the classical nucleation theory (CNT) has been found able to describe nucleation processes in phase transformations and crystallisation to a certain extent, but its predictive strength is very limited [1–3,5]. According to the CNT, the Gibbs free energy change ΔG during a homogenous nucleation event is given by:

$$\Delta G = -V\Delta g_V + A\gamma \quad (1)$$

in which V is the volume of the nucleus, Δg_V is the Gibbs free energy difference between the parent and product phases per unit of volume, A is the area of the interface forming during the nucleation process and γ is the interfacial free energy per unit area of the created interface [6]. In recent years, the universal applicability of the CNT has been questioned in the field of nanoscience and nanotechnology, where nonclassical nucleation mechanisms have been proposed, indicated as “aggregation of nuclei” (or “coalescence of nuclei”) and “stepwise nucleation” [3,7 12]. Schematics of the free-energy change ΔG with the evolution of the nucleus by different pathways, classical and nonclassical, are indicated in Fig. 1a c. When the two nonclassical mechanisms take place simultaneously during the nucleation of a new phase [7], it is assumed that the corresponding schematic evolution of ΔG can be illustrated as in Fig. 1d, which will be discussed in the present paper. The nonclassical nucleation mechanisms have mainly been studied for crystallisation processes in solutions or colloids [7,8], with a limited number of studies focusing on solid-solid phase transformations [3]. Further investigations are required to determine whether nonclassical nucleation processes can take place in solid-solid phase transformations.

Regardless of the long history of experimental and theoretical studies [13,14], nucleation processes during solid-solid phase transformations are still poorly understood due to the experimental difficulty of observing small nuclei in bulk materials [1 3]. In the present paper, homogenous nucleation of the bcc phase in fcc iron is studied by molecular dynamics (MD) simulation. Understanding homogeneous nucleation, although often less abundantly occurring than heterogeneous nucleation in real materials, opens the way to fundamental knowledge on nucleation [15], which also forms the basis for heterogeneous nucleation of a new phase at defects, such as grain boundaries [16]. Besides the analysis of atomic configurations, in the present study the energetics of nucleation and initial growth of the bcc nuclei are investigated in relation to Fig. 1. Significant shortcomings in the fit for the CNT are observed, lead-

* Corresponding author.
E-mail address: Xiaoqin.Ouyang@csu.edu.cn (X. Ou).

https://doi.org/10.1016/j.actamat.2022.117655
1359-6454/

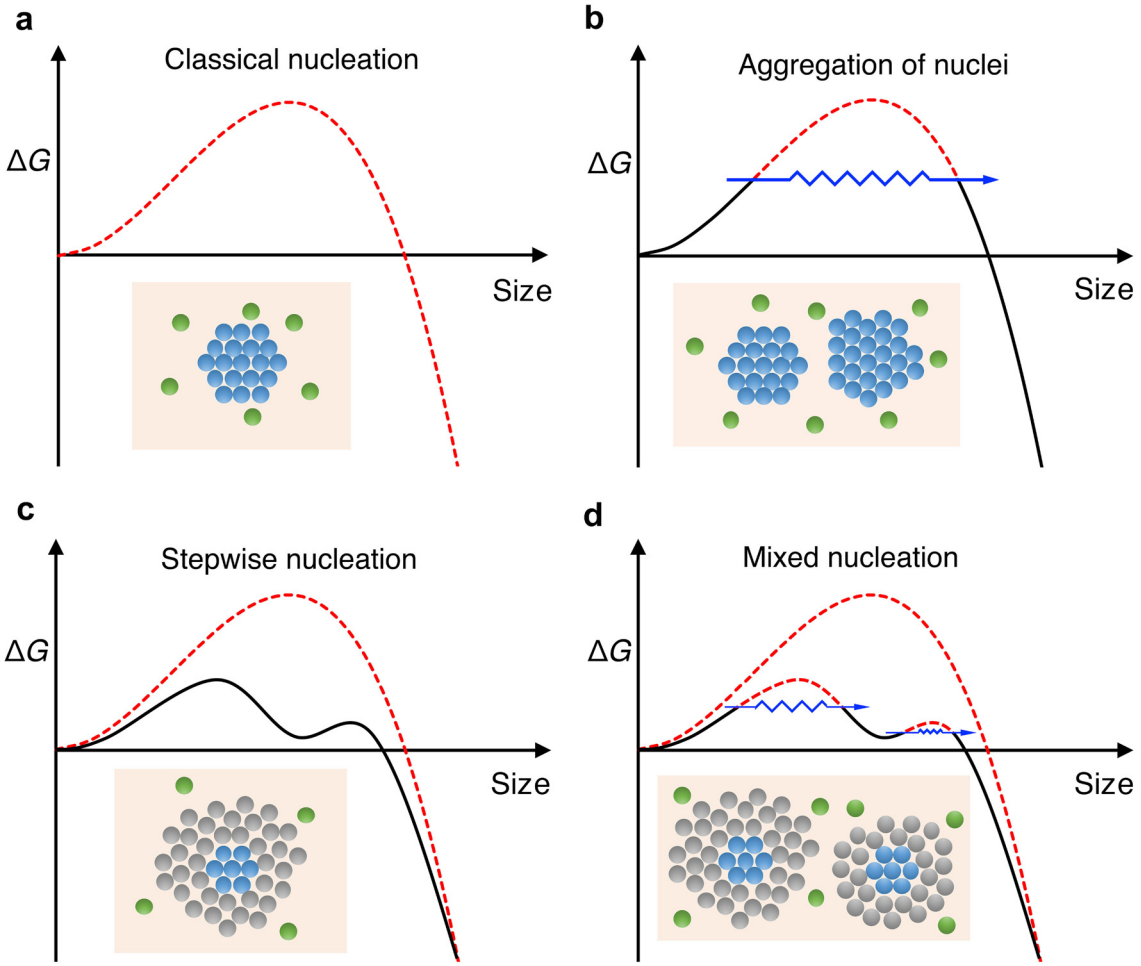

Fig. 1. Schematic of the free-energy change due to nucleation ΔG with the evolution of the nucleus by different pathways. (a) Classical nucleation through atom-by-atom addition [6,12]. ΔG goes through a maximum as a function of nucleus size. If a nucleus can overcome the energy barrier, it is stabilised and actually grows into a grain. (b) Nucleation by aggregation of subcritical clusters [8,10 12]. When two or more subcritical clusters merge to form a nucleus beyond the critical size, as marked by the blue arrow in (b), the free energy of the system decreases because a certain area of interface is eliminated. Thus, the nucleus is stabilised by aggregation by which the high-energy barrier is circumvented [8,10,11]. (c) Stepwise nucleation involving an intermediate state between the parent and product phases [3,9,12]. Formation of an intermediate state reduces the interfacial energy, thus the high-energy barrier for nucleation predicted by the CNT is replaced by lower energy barriers, as indicated by the black solid curves [3,9]. (d) Nucleation combining coalescence of subcritical clusters and stepwise nucleation. The free energy change due to nucleation follows both nonclassical pathways in a complementary way, as indicated by the solid curves in (d). Colours of atoms in the inserts in (a d) represent phase structures: green-parent phase; grey-intermediate state; blue-product phase. The dashed red curves predicted by the CNT are avoided by nonclassical nucleation pathways in (b d).

ing to the conclusion that alternative mechanisms occur during nucleation. The occurrence of nonclassical nucleation mechanisms is then explored and discussed with regard to their role in the stabilisation of a bcc nucleus during the fcc-to-bcc phase transformation.

2. Methods

In the present work, the embedded-atomic method (EAM) potential from Mendelev et al. [17] is used, which describes the stable ferromagnetic bcc phase. To investigate the homogeneous nucleation of one bcc particle, it is required that there is enough distance between the nucleus and its neighbours to avoid their interaction influencing the process. For the Mendelev potential, no phase transformation occurs in the fcc crystal at or below 100 K while the fcc structure does transform to the bcc structure at or above 150 K [18]. At a temperature of 200 K or higher, the density of bcc nuclei is very high due to the small energy barrier for the fcc-to-bcc transformation along the Bain path ($\Delta E_{Bain} < 1$ meV) based on the Mendelev potential [19]. The bcc nuclei grow into contact with its neighbours very fast, which makes it difficult to analyse the homogeneous nucleation process. Comparatively, only three stable bcc nuclei that are at an appreciable mutual distance form inside the fcc crystal at 160 K, which enables the possibility to track the nucleation process of an individual bcc nucleus without the influence from its neighbouring nuclei (see Fig. 2). Therefore, the temperature is fixed at 160 K in the present study, which provides a proper magnitude of the driving force for the homogeneous nucleation of bcc particles in view of the short simulation times.

One cubic simulation system with fcc single crystal is studied with the *x*, *y* and *z* axes parallel to the $[1\ 0\ 0]_{fcc}$, $[0\ 1\ 0]_{fcc}$ and $[0\ 0\ 1]_{fcc}$ directions, respectively. The system is built with 864,000 atoms in a box of $60 \times 60 \times 60$ fcc unit cells ($\mathbf{219.48} \times \mathbf{219.48} \times \mathbf{219.48}$ Å^3). The lattice parameter for the fcc crystal is 3.658 Å. The simulation is performed using a barostat and a thermostat of the Nosé-Hoover type (NPT ensemble) at a constant temperature of 160 K under a constant pressure of 100,000 Pa. Periodic boundary conditions are employed in the *x*, *y* and *z* directions. The simulation involves 10,000 steps with a time step of 0.5 fs. Calculations are performed with the open-source LAMMPS code [20]. The adap-

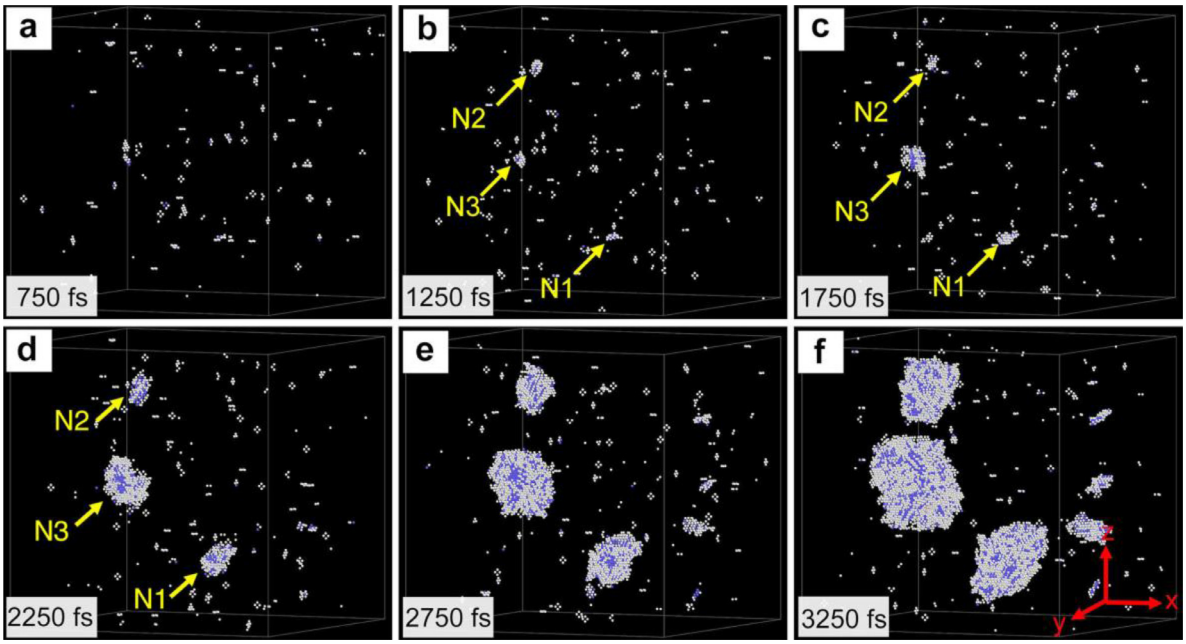

Fig. 2. Configurations of bcc nucleation at 160 K. Colours of atoms represent phase structures: blue-bcc; white-unidentified. Atoms in the fcc structure are not displayed.

tive common neighbour analysis (a-CNA) [21] is used to determine atoms as belonging to either the fcc, hcp, bcc phase or remaining unidentified. The configurations are displayed using the software OVITO [22]. The method of the thermodynamic analysis of the nucleation process during phase transformation is included in the supplementary materials.

3. Results and discussion

3.1. MD simulation of the bcc nucleation

MD simulation in Fig. 2 shows that homogeneous nucleation of the bcc phase takes place in the fcc iron at 160 K. In Fig. 2 all atoms with the fcc structure have been removed. The largest three bcc nuclei are labelled by the yellow arrows as N1, N2 and N3. In the present study, the bcc nuclei N1 and N2, which provide fundamental information on nucleation mechanisms, are chosen as representative for the process and are extensively discussed in the following sections. Details regarding the evolution of nucleus N3 are included in the supplementary information.

Besides the atoms in the bcc structure, a number of atoms, which are neither in the fcc nor the bcc structure and therefore unidentified by the a-CNA method [21], are present around the nucleus clusters, as shown in Fig. 2. One reason for atoms to have an unidentified structure may be that those atoms are located at the bcc/fcc phase interfaces, where the local structure is neither the one nor the other. Another reason may be that the atoms with unidentified structure are not in the crystallographic configuration of either the bcc or fcc lattice, but form an intermediate state.

3.2. Analysing nucleation of bcc phase from fcc bulk in the CNT framework

We employ the mathematical expression of the CNT to study the homogeneous nucleation process at the atomic scale in MD simulations. By incorporating an effective size d ($d = V^{1/3}$) of a nucleus into Eq. (1), the CNT can be interpreted in MD simulations with the expression:

$$\Delta G = -d^3 \Delta g_V + f d^2 \gamma \tag{2}$$

where Δg_V is the potential energy difference per unit volume between the fcc and bcc phase, f is the shape parameter of the nucleus ($f = A/V^{2/3}$) and γ is the interfacial energy (the detailed derivation process is included in the Supplementary Materials, which shows that ΔG can be represented by the potential energy change ΔU with good accuracy). The nucleus will be considered as either existing of atoms in a bcc structure only or existing of bcc atoms and unidentified atoms. The effective nucleus size is calculated as $d_i = V_i^{1/3}$, with i being the structure of the atoms considered in the calculation of this size. Thus, d_{bcc} considers only the atoms that are identified as bcc and $d_{\mathrm{bcc+uni}}$ considers also the unidentified atoms to be part of the nucleus. The free energy change ΔG is plotted as a function of the size of each individual nucleus forming inside the fcc crystal in Fig. 3 and Fig. A1. It should be noted that the contribution of elastic strain energy, which ranges from 0.00044 to 0.00066 eV/Å^3 [23,24], to the non-chemical driving force is neglected in Eq. (2), because it is too small compared with the chemical driving force Δg_V (equalling to 0.01013 eV/Å^3) at the low temperature of 160 K to have a significant effect on the process.

Regardless of fluctuations, the energy change due to a nucleation event initially shows an overall increasing trend and then decreases with increasing nucleus size. The energy change ΔG is fitted as a function of the size d_{bcc} according to Eq. (2) (the red curves in Fig. 3a,b and Fig. A1), in which Δg_V is taken equal to the value resulting from the potential ($\Delta g_V = 10.13$ meV/Å^3). It is seen that the CNT reasonably describes the energy change during the stable stage of the nucleus, i.e. the initial growth period. However, it predicts a high activation energy for nucleation (see inserts in Fig. 3a,b and Fig. A1), which is not followed by the nucleus energy. This will be discussed in more detail in the following section. Fitting to different values of the size range d_{bcc} does not result in a better match between the model curves and the thermodynamic data points. In order to make optimal use of the available data, the fits have been performed over the maximum range of d_{bcc}. The

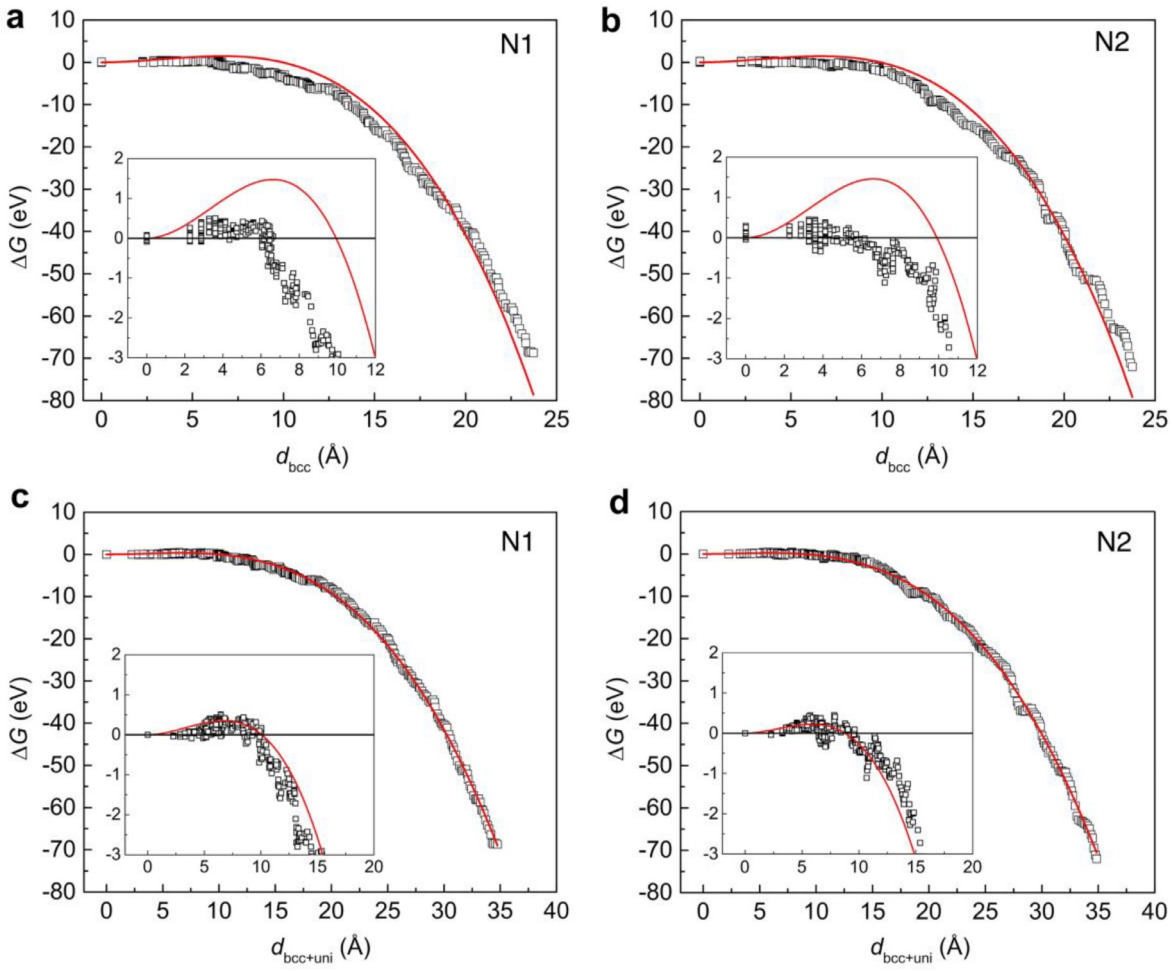

Fig. 3. Plots of the energy change as a function of nucleus size from MD simulation and based on CNT. (a d) Energy change for nucleus N1(a,c) and nucleus N2 (b,d). The energy change for nucleus N3 is given in Fig. A1. The size d_{bcc} in (a) and (b) only considers atoms in the bcc structure, while the size $d_{bcc+uni}$ in (c) and (d) involves atoms in both the bcc and unidentified structures. The inserts in (a d) are the enlarged views of the nucleation stage for each individual nucleus. The black open dots represent the thermodynamic MD-data. MD-data in (a) and (b) is fitted according Eq. (2) with fixed Δg_V=10.13 meV/Å^3 (red curves), while that in (c) and (d) is fitted according Eq. (2) without fixing Δg_V.

bcc nuclei N1, N2 and N3 reach the size of approximately 28.0 Å, 23.8 Å and 38.2 Å, respectively, at around 3250 fs, after which the nuclei grow into contact with each other. Thus $d_{bcc} = 23.8$ Å is chosen as the cutoff of the fitting range. The only fitting parameter is the product $f\gamma$, the coefficient of the quadratic term in Eq. (2), which is represented in Supplementary Table A1. Note that these parameter values do have a realistic meaning, since the initial growth stage is, contrary to the nucleation stage, accurately described.

Approximately the same values for the fitting parameter (the product $f\gamma$) are obtained for the three nuclei (Table A1). Based on the product $f\gamma$, the interface energy γ can be estimated for a nucleus with a specific shape parameter f. From the analysis of the atomic configurations it follows that the nuclei have an ellipsoidal morphology with an average shape parameter $f \approx 12$ (Fig. A2). The interface energy is therefore approximately 134 to 139 mJ/m^2 for the bcc nuclei (Table A1). It has been reported that coherent phase interfaces in metals and alloys have an interface energy less than 200 mJ/m^2, while semi-coherent interfaces have an energy in the range of 200 to 500 mJ/m^2 [3,25]. The low interface energy of less than 150 mJ/m^2 thus indicates coherency between the nucleus and the fcc phase, which can be seen from the alignment of atoms in the bcc nucleus and fcc phase on a monolayer of the $(1\ \bar{1}\ 0)_{fcc}$ plane for N1, N2 and N3 (Fig. A2).

Fig. 3 shows that the nucleus enters the range of stable growth at a size of 6 to 7 Å, which corresponds to approximately 20 to 30 atoms in the critical bcc nucleus (Table A1). Offerman et al. [1] used X-ray diffraction at a synchrotron source to study the heterogeneous nucleation rate of ferrite grains as a function of temperature during the austenite-to-ferrite transformation in steel. Based on the CNT these authors estimated the critical ferrite nucleus to consist of 10 to 100 atoms. From our MD simulation it results that the energy barrier is largely overestimated by the CNT, as shown by the inserts in Fig. 3a and 3b. Offerman et al. [1] found experimental values for the activation energy for nucleation that are also far lower than predicted by the CNT assuming any conceivable nucleus shape.

However, when the unidentified atoms are considered as part of the nucleus, it is seen that the calculated energy barrier from the fitting curves decreases to a value ranged between 0.22 and 0.35 eV with the fitting driving force Δg_V between 2.13 and 2.32 meV/Å^2 (Fig. 3c,d, Fig. A1 and Table A2). This implies that the presence of unidentified atoms as part of the bcc nuclei decreases the driving force, because the unidentified atoms have higher potential energy than the atoms with bcc structure. Nevertheless, they ap-

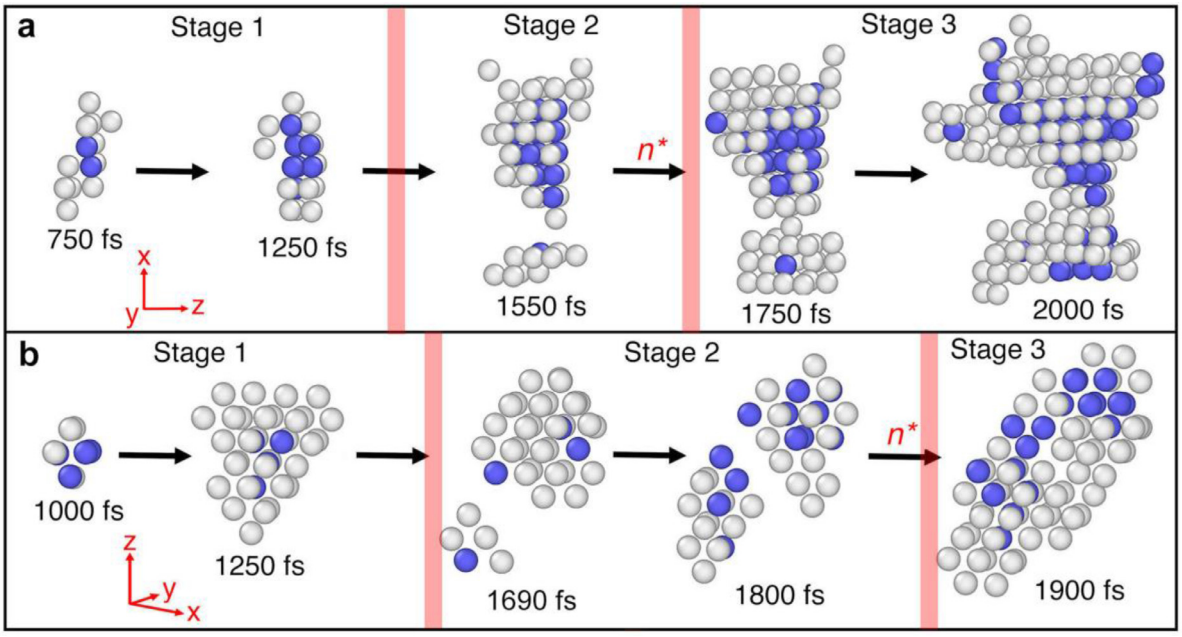

Fig. 4. Nucleation process by aggregation of neighbouring clusters. (a,b) Nucleation process for nucleus N1(a) and nucleus N2 (b) (nucleus N3 in Fig. A3). n^* represents the occurrence of the critical nucleus size. Colours of atoms represent different phase structures: blue-bcc; white-unidentified. Atoms in the fcc structure are not displayed in (a) and (b).

pear to play a crucial role in the nucleation process, as will also be discussed later. Additionally, the MD simulations by Song and Hoyt [26,27] suggest the probability of the barrier-free nucleation events besides the classical nucleation events during the solid-solid fcc→bcc transformation initiating from grain boundaries in pure Fe. Their results present an activation energy lower than 0.068 eV for the barrier-free case and an activation energy ranging from 1 to 6 eV for the classical nucleation case [26 28]. The magnitude of the energy barrier for the homogeneous martensitic nucleation in the present study lies in between that for the barrier-free nucleation case and the classical nucleation case in Fe [26 28]. This consistency further reflects the reliability of the relatively low nucleation energy barrier obtained in the current simulation compared to that estimated from the CNT.

As explained, the energy barrier for homogenous nucleation is overestimated by the CNT. It is shown that the CNT describes the growth period of a postcritical nucleus but not its nucleation stage (Fig. 3a,b). Therefore, the calculated activation energy is not relevant for the nucleation process in the MD simulation. Since the CNT, which does not consider the unidentified atoms, fails to describe the bcc nucleation events, alternative interpretations will be discussed in the following section.

3.3. Nonclassical nucleation of bcc phase

As shown in the inserts of Fig. 3a,b, the CNT strongly overestimates the energy barrier to form a stable nucleus. In the view of the CNT, the bcc nucleus grows through atom-by-atom addition and develops with a distinct shape and well-defined, sharp bcc/fcc interfaces separating the product bcc phase and the parent fcc phase. Reality is, however, more complex. The simulations show that in the nucleation stage atoms in the bcc structure are located in several clusters, with unidentified atoms linking them into a single nucleus (Fig. 4). Therefore, the shape and size of the nucleus are not unambiguously defined. This complexity in the nucleation behaviour is not captured by the CNT. In fact, with this more complex behaviour the system chooses a lower-energy route in the nucleation event, circumventing the high activation energy predicted by the CNT. This section describes the homogeneous nucleation of bcc phase in the frame of nonclassical nucleation mechanisms.

3.3.1. Coalescence of subcritical clusters

During the nucleation of colloidal nanoparticles in solutions [8 10,29], aggregation of nearby subcritical clusters has been observed to play an important role in the formation of a stable nucleus. Similarly, aggregation of nearby subcritical clusters is observed in the formation of a stable bcc nucleus in the present MD simulation (Fig. 4 and Fig. A3). The interaction of two neighbouring subcritical clusters enables the survival of both. In this process, the two clusters combine, effectively forming a larger nucleus, which leads to stability. This can take place regardless of whether the two clusters have the same crystallographic orientation or not (Fig. 5). Identical orientations of neighbouring subcritical clusters lead to a single-crystalline nucleus after aggregation. Otherwise a bcc/bcc grain boundary forms inside the obtained aggregate but still the overall interfacial energy is lowered by the aggregation process.

Each bcc nucleus initiates with a single subcritical cluster. This primary cluster is variable in size and morphology before reaching the critical size. During the nucleation process, the number of atoms in the cluster fluctuates (Fig. A4). In addition, there are small neighbouring clusters forming and disappearing around the primary cluster. In the present paper, we focus on the period in which nuclei are stabilised by aggregation of the primary cluster and a neighbouring subcritical cluster (Fig. 6a,b and Fig. A5). The nucleation process is thus divided into three stages (Fig. 4 and Fig. A3). The schematic picture illustrating stages 1 to 3 is given in Fig. 6c. Stage 1 represents the period before the formation of the neighbouring subcritical cluster close to the primary cluster. At Stage 2, the neighbouring subcritical cluster forms near the primary one. At Stage 3, the primary subcritical cluster aggregates with the neighbouring subcritical cluster to form a larger cluster.

Due to this aggregation, the energy change caused by the formation of the combined nucleus decreases to a negative value with

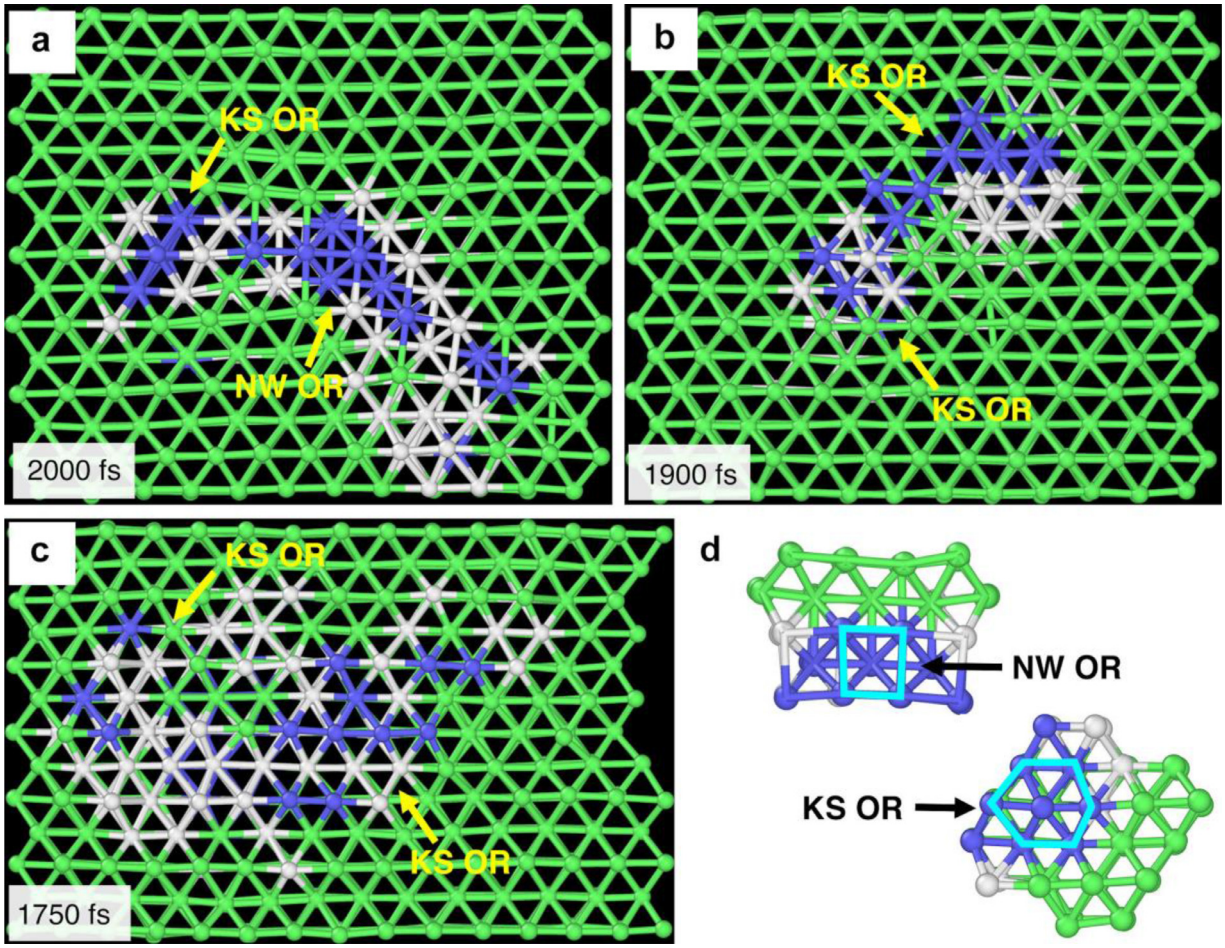

Fig. 5. The orientation of the aggregated clusters for nuclei: (a) N1, (b) N2 and (c) N3. For nucleus N1, one subcritical cluster has the Nishiyama-Wassermann (NW) orientation relationship (OR) [30] with the fcc phase, while its neighbour has the Kurdjumov-Sachs (KS) OR [31]. Due to their different ORs, a bcc/bcc grain boundary forms inside the obtained aggregate. For nucleus N2 however, the two subcritical clusters merge into a single nucleus after aggregation, because they have the same crystallographic orientation, the KS OR with the fcc phase. For nucleus N3, both clusters also have the KS OR with fcc, but in different variants, leading to a bcc/bcc grain boundary inside the aggregate. Illustration of the NW and KS OR are highlighted in light blue in (d). The view direction is parallel to $[1\ \bar{1}\ 0]_{fcc}$. Bonds are created between atoms within the cutoff distance of 3.2 Å. Colours of atoms represent different phase structures: blue-bcc; green-fcc; white-unidentified.

respect to the initial fully fcc state (Fig. 6a,b and Fig. A5,A6). In other words, the aggregation with a neighbouring subcritical cluster stabilises the primary cluster by overcoming an energy barrier that is much lower than predicted by the CNT. The number of atoms in the nucleus monotonically grows after aggregation, i.e. when entering into stage 3 (Fig. A4). The bcc nuclei are stabilised by effectively increasing in size and reducing the interfacial energy by aggregation, which circumvents the necessity to overcome the high energy barrier for the homogeneous nucleation envisaged by the CNT [7,29]. This explains the energy barrier being lower than the one predicted by the CNT for the bcc nuclei (Fig. 3a,b, Fig. 6 and Fig. A1,A5).

Besides the eventually stable nuclei, there are a number of bcc nuclei that fail to reach the critical size: they disappear. The number of atoms in such nuclei reaches a maximum of about 20 atoms in the unidentified and bcc structures, which then gradually diminishes if no aggregation with neighbouring subcritical clusters takes place. Therefore, it is deduced that bcc nuclei fail to surpass the critical size through atom-by-atom addition, as envisaged by the CNT. The aggregation of neighbouring subcritical clusters provides the opportunity for the primary cluster to reach and surpass the critical size and to circumvent the high CNT-predicted energy barrier for homogeneous nucleation.

Besides, previous literature by Olson and Cohen [23] also mentioned that coherent nucleation of the bcc structure from the fcc phase is thermodynamically impossible, because the elastic strain energy is an order of magnitude higher than the chemical free-energy change when the martensitic transformation occurs in ferrous alloys. Nonetheless, the elastic strain energy can be reduced significantly provided that the nucleus is made semicoherent by an array of anticoherency dislocations (or misfit dislocations). Similarly, in the present study the subcritical bcc nuclei form inside the fcc crystal due to thermal fluctuation, which involves homogeneous deformation and the formation of coherent interfaces between the subcritical bcc nuclei and the parent fcc crystal. This can be seen from the disordered atomic displacements for individual subcritical bcc nucleus in Fig. A7 (b, e, h). As a contrast, the coherent bcc/fcc interfaces for an individual subcritical bcc nucleus evolve into semicoherent bcc/fcc interfaces in the NW/KS OR for the corresponding postcritical bcc nucleus (Fig. 5). This can be seen from the shear movement of the $\{111\}_{\mathrm{fcc}}$ invariant plane by the slip of $\frac{a}{6}\langle 112\rangle$ Shockley partial dislocations at the bcc/fcc interface in Fig. A7 (c, f, i). Additionally, the simulation results in the present paper indicate that the CNT overestimates the energy barrier for the martensitic nucleation, which may be partially attributed to the coherency conversion of the interfaces during the nucleation

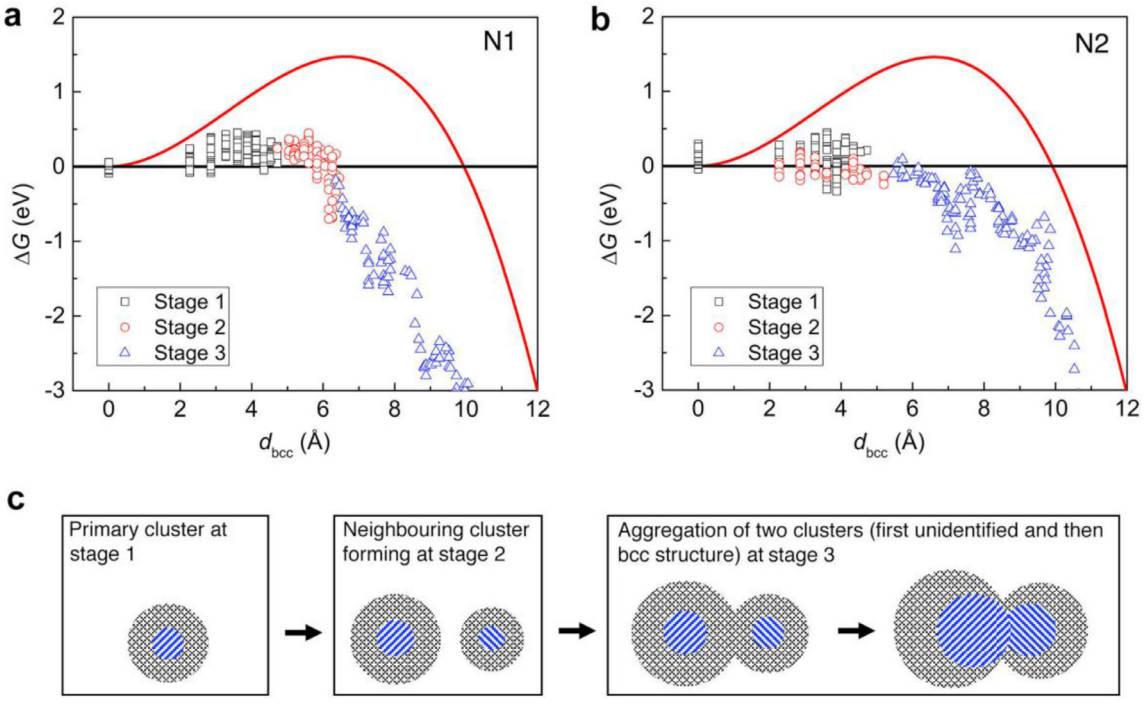

Fig. 6. The energy change as a function of the nucleus size at different stages for bcc nuclei. (a,b) The energy change of nucleus N1 (a) and nucleus N2 (b). The energy change of nucleus N3 is in Supplementary Fig. A5. The red line indicates the fit according to the CNT, also shown in Fig. 3(a,b). (c) The scheme illustrates the three stages (see Fig. 4) in (a) and (b). The energy change ΔG involves the atoms in both the bcc and unidentified structures, which correspond to the blue and grey regions in (c). The energy change ΔG at stage 1 and 2 is only contributed to by the primary cluster while that at stage 3 is contributed to by the aggregate.

process. The coalescence of two neighbouring subcritical bcc nuclei may account for the introduction of extra lattice dislocations that dissociate into $\frac{a}{6}\langle 112\rangle$ Shockley partial dislocations. The movement of the partial dislocations then converts the coherent interface to a semicoherent one. As a result, the elastic strain energy of the initially fully coherent interface is reduced and the bcc nucleus is stabilized.

3.3.2. Stepwise nucleation

The bcc nuclei are composed of a core consisting of atoms in a bcc structure surrounded by a number of unidentified atoms (Fig. 2,4,5 and Fig. A3). The unidentified atoms do not only act as the interfaces dividing the fcc and bcc structures, but also as an intermediate phase existing between the clusters, which will be discussed later in this section. Note that the unidentified atoms extend over a distinctly broader range than can be envisaged for an interface (Fig. 4,5 and Fig. A3). In a later stage, they bind the distinct bcc clusters to form a single nucleus.

The energy change of individual bcc nuclei in Fig. 6 is contributed to by both the bcc and unidentified atoms (Fig. A5). Regardless of local fluctuations, the energy change of the unidentified structure goes through a maximum value first, which is followed by a maximum for the bcc structure for each nucleus (Fig. 7 and Fig. A8,A9). Both maxima are much lower than predicted by the CNT. Furthermore, the energy change of each of the three nuclei N1, N2, N3 is dominated by that of the unidentified atoms. Thus, it is inferred that the nucleation of the bcc phase in the fcc bulk essentially follows a stepwise "fcc → intermediate → bcc" process instead of a single-step "fcc → bcc" transformation. This is similar to the role of metastable intermediate phases in many precipitation sequences. The fcc phase transforms into the metastable intermediate state first, because of the lower barrier for its nucleation than the direct nucleation of the stable bcc phase. By using single-particle-resolution video microscopy of colloidal films of diameter-tunable microspheres, Peng et al. [3] also found a two-step nucleation process with an intermediate liquid forming during solid-solid phase transitions. In our case, the unidentified structure that acts as the shell of the core bcc structure is similar to such an intermediate state.

Peng et al. [3] proposed two low energy barriers for the two-step nucleation during the solid-solid phase transitions, based on the Ostwald step rule. The first refers to the barrier for the nucleation of the intermediate state in the parent solid phase and the second for the nucleation of the product solid from the generated intermediate state. This is similar to the nucleation during precipitation sequences in the solid state [12]. Also in the present study the high energy barrier of homogeneous nucleation predicted by the CNT is replaced by two lower energy barriers (Fig. 7c). Since the stepwise nucleation coincides with the aggregation of subcritical clusters, the overall energy change during the nucleation process becomes more complex. The energy change of the nucleus exhibits the characteristics as proposed in the schematic picture in Fig. 1d when both nonclassical nucleation mechanisms take place simultaneously during the nucleation event.

4. Conclusion

The present research pioneers in the analysis of the mechanisms involved in homogeneous nucleation by molecular dynamics simulations, for the particular case of nucleation of bcc phase in a fcc matrix in pure iron. Our investigations show that the high energy barrier predicted by the classical nucleation theory can be circumvented by nonclassical nucleation mechanisms such as step-wise nucleation and aggregation of subcritical clusters. These mechanisms have been originally reported for nucleation in crystallisation processes in solutions or colloids. In the present study they are for the first time shown to be a nucleation process in physically simulated solid-solid phase transformations. Their occur-

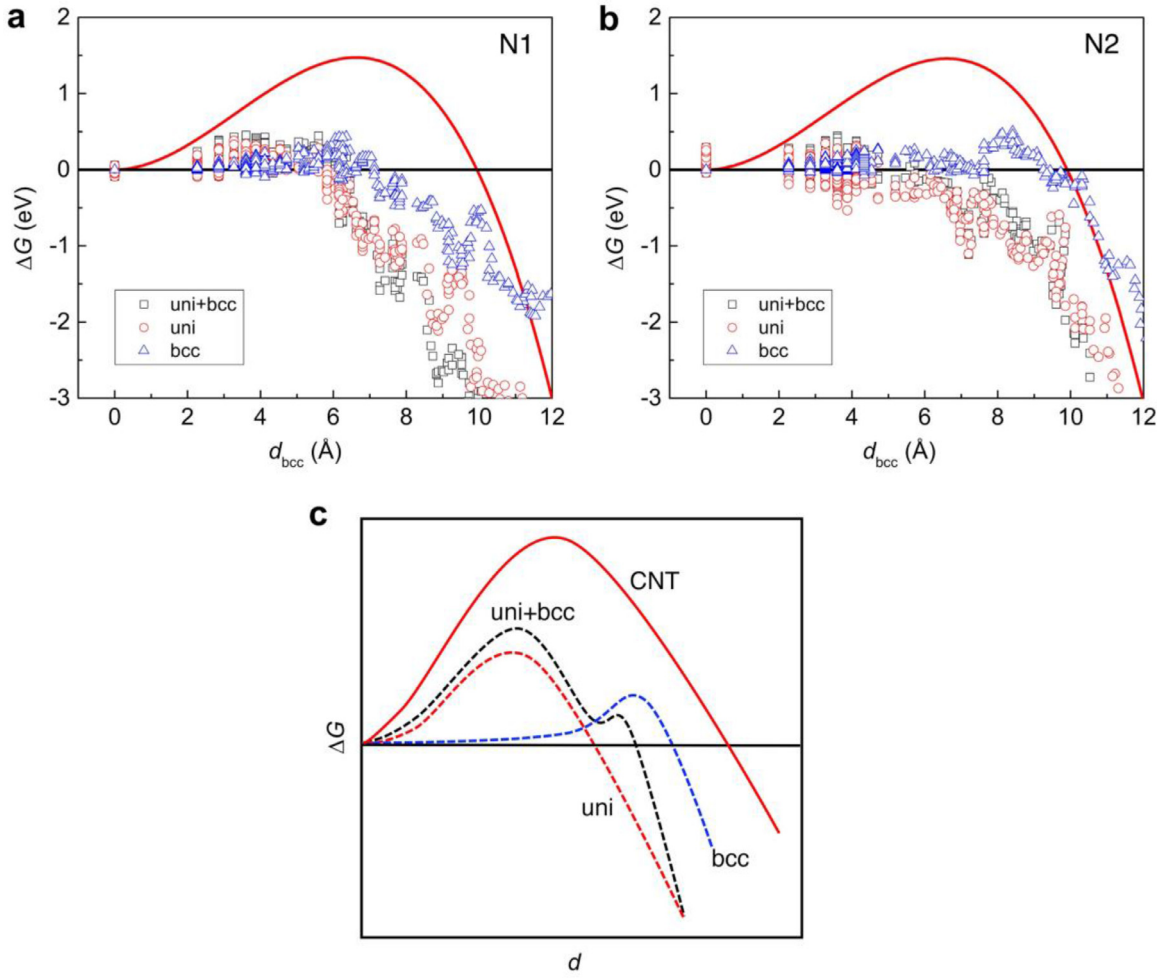

Fig. 7. Contributions of different structures to the energy change of bcc nuclei. (a,b) Contributions of the bcc (blue triangles) and unidentified (red circles) structures to the energy change of the bcc nuclei (black squares) as a function of the nucleus size: (a) N1, (b) N2 (N3 in Fig. A8). The solid red curves in (a) and (b) show the prediction by the CNT. (c) Schematic picture of the energy change ΔG in (a) and (b). The labels "uni" and "bcc" in (a c) represent unidentified and bcc structures (For interpretation of the references to color in this figure legend, the reader is referred to the web version of this article.).

rence explains low values of the nucleation barrier in solid-state transformations, which have been experimentally observed in the past. This study shows the complexity, but also the versatility of solid-state nucleation processes.

Declaration of Competing Interest

The authors declare that they have no known competing financial interests or personal relationships that could have appeared to influence the work reported in this paper.

Acknowledgments

The authors would like to thank Prof. Barend J. Thijsse and Assoc. Prof. S. Erik Offerman from Delft University of Technology, the Netherlands for the fruitful discussions. The research leading to these results has received funding from the European Research Council under the European Union's Seventh Framework Programme FP7/2007–2013/ERC [grant number 306292] and National Natural Science Foundation of China (grant number 51901248).

Supplementary materials

Supplementary material associated with this article can be found, in the online version, at doi:10.1016/j.actamat.2022.117655.

References

[1] S.E. Offerman, N.H. van Dijk, J. Sietsma, S. Grigull, E.M. Lauridsen, L. Margulies, H.F. Poulsen, M. Th. Rekveldt, S. van der Zwaag, Grain nucleation and growth during phase transformations, Science 298 (2002) 1003–1005.
[2] N.H. Van Dijk, S.E. Offerman, J. Sietsma, S. van der Zwaag, Barrier-free heterogeneous grain nucleation in polycrystalline materials: the austenite to ferrite phase transformation in steel, Acta Mater. 55 (2007) 4489–4498.
[3] Y. Peng, F. Wang, Z. Wang, A.M. Alsaye, Z. Zhang, A.G. Yodh, Y. Han, Two-step nucleation mechanism in solid-solid phase transitions, Nat. Mater. 14 (2015) 101–108.
[4] A. Gamboa, B. Farbos, P. Aurel, G.L. Vignoles, J.M. Leyssale, Mechanism of strength reduction along the graphenization pathway, Sci. Adv. 1 (2015) e1501009.
[5] L.Y. Yu, M.R. Niazi, G.O. Ngongang Ndjawa, R. Li, A.R. Kirmani, R. Munir, A.H. Balawi, F. Laquai, A. Amassian, Programmable and coherent crystallization of semiconductors, Sci. Adv. 3 (2017) e1602462.
[6] J.W. Christian, The Theory of Transformations in Metals and Alloys, Pergamon, Oxford, 1981.
[7] J. Lee, J. Yang, S.G. Kwon, T. Hyeon, Nonclassical nucleation and growth of inorganic nanoparticles, Nat. Rev. Mater. 1 (2016) 16034.
[8] J. Park, H. Elmlund, P. Ercius, J.M. Yuk, D.T. Limmer, Q. Chen, K. Kim, S.H. Han, D.A. Weitz, A. Zettl, A.P. Alivisatos, 3D structure of individual nanocrystals in solution by electron microscopy, Science 349 (2015) 290–295.
[9] S.Y. Chung, Y.M. Kim, J.G. Kim, Y.J. Kim, Multiphase transformation and Ostwald's rule of stages during crystallization of a metal phosphate, Nat. Phys. 5 (2009) 68–73.
[10] H.M. Zheng, R.K. Smith, Y. Jun, C. Kisielowski, U. Dahmen, A.P. Alivisatos, Observation of single colloidal platinum nanocrystal growth trajectories, Science 324 (2009) 1309–1312.

[11] Z.R. Wang, F. Wang, Y. Peng, Z.Y. Zheng, Y.L. Han, Imaging the homogeneous nucleation during the melting of superheated colloidal crystals, Science 338 (2012) 87–90.
[12] J.J. De Yoreo, P.U.P.A. Gilbert, N.A.J.M. Sommerdijk, R.L. Penn, S. Whitelam, D. Joester, H.Z. Zhang, J.D. Rimer, A. Navrotsky, J.F. Banfield, A.F. Wallace, F.M. Michel, F.C. Meldrum, H. Cölfen, P.M. Dove, Crystallization by particle attachment in synthetic, biogenic, and geologic environments, Science 349 (2015) aaa6760.
[13] H.I. Aaronson, W.F. Lange III, G.R. Purdy, Discussion to “Grain nucleation and growth during phase transformations” by S.E. Offerman et al., Science, 298, 1003 (November 1, 2002), Scripta Mater. 51 (2004) 931–935.
[14] W.F. Lange III, M. Enomoto, H.I. Aaronson, The kinetics of ferrite nucleation at austenite grain boundaries in Fe-C alloys, Metall. Trans. A 19 (1988) 427–440.
[15] B.J. Wang, H. Urbassek, Phase transitions in an Fe system containing a bcc/fcc phase boundary: an atomistic study, Phys. Rev. B 87 (2013) 104108.
[16] Y. Peng, W. Li, F. Wang, T. Still, A.G. Yodh, Y.L. Han, Diffusive and martensitic nucleation kinetics in solid-solid transitions of colloidal crystals, Nat. Comm. 8 (2017) 14978.
[17] M.I. Mendelev, S. Han, D.J. Srolovitz, G.J. Ackland, D.Y. Sun, M. Asta, Development of new interatomic potentials appropriate for crystalline and liquid iron, Phil. Mag. 83 (2003) 3977–3994.
[18] X. Ou, M. Song, Deformation mechanisms of mechanically induced phase transformations in iron, Comput. Mater. Sci. 162 (2019) 12–20.
[19] M. Müller, P. Erhart, K. Albe, Analytic bond-order potential for bcc and fcc iron – comparison with established embedded-atom method potentials, J. Phys. Condens. Matter. 19 (2007) 326220.
[20] S. Plimpton, Fast parallel algorithms for short-range molecular dynamics, J. Comp. Phys. 117 (1995) 1–19 http://lammps.sandia.gov/. Accessed on August 1th, 2021.
[21] A. Stukowski, Structure identification methods for atomistic simulations of crystalline materials, Modell. Simul. Mater. Sci. Eng. 20 (2012) 045021.
[22] A. Stukowski, Visualization and analysis of atomistic simulation data with OVITO-the open visualization tool, Modell. Simul. Mater. Sci. Eng. 18 (2010) 015012.
[23] G.B. Olson, M. Cohen, A perspective on martensitic nucleation, Metall. Trans. A 7a (1976) 1905–1976.
[24] Q. Luo, H. Chen, W. Chen, C. Wang, W. Xu, Q. Li, Thermodynamic prediction of martensitic transformation temperature in Fe-Ni-C system, Scripta Mater. 187 (2020) 413–417.
[25] D.A. Porter, K.E. Easterling, M.Y. Sherif, Phase Transformations in Metals and Alloys, 3, CRC Press, UK, 2008.
[26] H. Song, J.J. Hoyt, Barrier-free nucleation at grain-boundary triple junctions during solid-state phase transformations, Phys. Rev. Lett. 117 (2016) 238001.
[27] H. Song, J.J. Hoyt, A molecular dynamics study of heterogeneous nucleation at grain boundaries during solid-state phase transformations, Comput. Mater. Sci. 117 (2016) 151–163.
[28] H. Song, R. Shi, Y. Wang, J.J. Hoyt, Simulation study of heterogeneous nucleation at grain boundaries during the austenite-ferrite phase transformation: comparing the classical model with the multi-phase field nudged elastic band method, Metall. Mater. Trans. A 48 (2016) 2730–2738.
[29] J. Baumgartner, A. Dey, P.H.H. Bomans, C.Le Coadou, P. Fratzl, N.A.J.M. Sommerdijk, D. Faivre, Nucleation and growth of magnetite from solution, Nat. Mater. 12 (2013) 310–314.
[30] Z. Nishiyama, X-ray investigation of the mechanism of the transformation from face-centred to body-centred cubic lattice, Sci. Rep. Tohoku Imp. Univ. 23 (1934) 637–664 Cited by M. G. Hall, H. I. Aaronson, K. R. Kinsman, The structure of nearly coherent fcc: bcc boundaries in a Cu-Cr alloy, Surf. Sci. 31 (1972) 257-274..
[31] G.V. Kurdjumov, G. Sachs, About the mechanism of steel hardening, Z. Phys. 64 (1930) 325–343 Cited by M. G. Hall, H. I. Aaronson, K. R. Kinsman, The structure of nearly coherent fcc: bcc boundaries in a Cu-Cr alloy, Surf. Sci. 31 (1972) 257-274.